Supplementary Information

Appendix A: Model description and parameter list

FORMIND is an individual-based, spatially explicit and process-based model designed to simulate the dynamics of species-rich forests (Fischer et al., 2016). The model simulates the processes of establishment, growth, competition and mortality of trees on a regular grid of patches with the dimensions of a typical treefall gap (20 m × 20 m). Within each patch, the trees do not have explicit spatial positions as with the gap-model concept (Shugart, 1984). By combining many patches, large forest areas up to hundreds of hectares can be simulated.

In each simulated time step (1 year), the following main processes take place: 1) Establishment: Seeds are distributed over the forest area. If light conditions are suitable, new saplings can establish and compete for light and space in the patch. 2) Competition: The main driving factor of the model is light. Radiation intensity within each patch decreases from the top to the ground according to a light extinction function. The light extinction depends on the combined vertical leaf area profile of all trees in the patch. The productivity of each tree is determined by the available light in its height layer. 3) The growth of each tree depends on its gross primary productivity (GPP), respiration and species-specific physiological and allometric parameters. 4) Mortality: Trees die stochastically according to a species-specific mortality rate. If a tree falls it can damage neighboring trees in adjacent patches.

Besides these core processes, FORMIND offers the following feature: Carbon Cycle: Gross primary production, respiration and net primary production are calculated for each individual tree. Based on this, the carbon balance for a whole forest can be derived, including soil respiration, deadwood respiration and net ecosystem productivity.

Tree species with similar ecological traits are aggregated into plant functional types (PFT) to facilitate parameterization for diverse forests and reduce computation time. The PFTs may represent different successional types (from pioneers to climax species) and size classes (from understory to emergent species).

FORMIND has been applied to various forest sites in Brazil, Ecuador, French Guyana, Germany, Madagascar, Malaysia, Mexico, Panama, Tanzania and Venezuela (Köhler & Huth, 1998; Kammesheidt et al., 2001; Huth et al., 2004; Dislich et al., 2009; Groeneveld et al., 2009; Dislich & Huth, 2012; Bohn et al., 2014; Kazmierczak et al., 2014; Pütz et al., 2014; Dantas de Paula et al., 2015; Fischer et al., 2015). The detailed model description was published with Fischer et al. (2016) and can also be found on www.formind.org. Parameters for the study site La Selva, Costa Rica are listed in Tab. A.1 and A.2.

Table A.1: General parameters and constants

	Parameter	Unit	Value	Reference
general	t_{end}	yr	1000	technical parameter
	t_y	yr	1	technical parameter
	A_{area}	ha	9	technical parameter
	A_{patch}	m^2	400	technical parameter
	MaxGrp		6	technical parameter
	Δh	m	0.5	technical parameter
carbon cycle	AET	mm yr^{-1}	1350	-
	$t_{Sslow \rightarrow A}$	yr^{-1}	1/750	14
	$t_{Sfast \rightarrow A}$	yr^{-1}	1/15	14

Table A.2: PFT-specific parameters

	Parameter	Unit	Plant functional type (PFT) 1	2	3	4	5	6	Reference
geometry	H_{max}	m	50	45	30	18	15	13	field data
	h_0		43.4						15,16
	h_1		0.6						15,16
	c_{l0}		0.4						15
	c_{d0}		18.16						15,16
	c_{d1}		0.68						15,16
	ρ	t_{ODM}/m^3	0.55	0.48	0.51	0.44	0.69	0.44	field data
	σ		0.7						15
	f_0		0.49						3
	f_1		-0.1						3
	l_0		2						15
	l_1		0						15
recruitment	N_{seed}	ha^{-1} yr^{-1}	17	18	350	25	29	421	Calibrated
	I_{seed}		0.02	0.07	0.47	0.04	0.25	0.02	10
	D_{min}	m	0.05						10
mortality	M_B	yr^{-1}	0.06	0.06	0.04	0.07	0.08	0.01	field data + calibrated
	f_{fall}		0.4						15,17
photosynthesis	I_0	μmol_{photon} m^{-2} s^{-1}	700						-
	k		0.7						5
	l_{day}	h	12						-
	ϕ_{act}	d	365						-
	p_{max}	μmol_{CO2} μmol_{photon}^{-1}	6.3	11.3	27.7	6.3	11.3	6.3	calibrated
	α	μmol_{CO2} m^{-2} s^{-1}	0.11	0.14	0.02	0.19	0.08	0.16	calibrated
growth	function		polynom (y = g0 + g1 d + g2 d^2 + g3 d^3)						
	g_0		0.0093	0.0148	0.018	0.024	-0.0339	-0.0056	field data
	g_1		0.0167	0.0547	0.0482	-0.2407	1.0413	0.1171	field data
	g_2		-0.0403	-0.1087	-0.216	1.2485	-7.1106	0.2962	field data
	g_3		0.0174	0.0433	0.1582	-2.4415	14.161	-4.703	field data

 Table A-3 Species Grouping into FORMIND PFTs

FORMIND PFT	CARBONO Code	Genus	Species
1	DENDARBO	Dendropanax	arboreus
1	GUARGENT	Guarea	gentryi
1	DIPTPANA	Dipteryx	panamensis
1	PROTPANA	Protium	panamense
1	DUSSMACR	Dussia	macroprophyllata
1	VITECOOP	Vitex	cooperi
1	PROTPITT	Protium	pittieri
1	MINQGUIA	Minquartia	guianensis
1	WARSCOCC	Warszewiczia	coccinea
1	ILEXSKUT	Ilex	skutchii
1	RAUVPURP	Rauvolfia	purpurascens
1	CARANICA	Carapa	nicaraguensis
1	PTERSP.A	Pterocarpus	sp. A
1	QUARBRAC	Quararibea	bracteolosa
1	OTOBNOVO	Otoba	novogranatensis
1	GUARHOFF	Guarea	hoffmanniana
1	ABARADEN	Abarema	adenophora
1	MACRCOST	Macrolobium	costaricense
1	ANDIINER	Andira	inermis
1	TABEARBO	Tabernaemontana	arborea
1	POUT1062	Pouteria	
1	CLETCOST	Clethra	costaricensis
1	POUTCALI	Pouteria	calistophylla
1	DUSSSP	Dussia	
1	OCOTFLOR	Ocotea	floribunda
1	HIEROBLO	Hieronyma	oblonga
1	GARCINTE	Garcinia	intermedia
1	THEOSIMI	Theobroma	simiarum
1	ESCHCOLL	Eschweilera	collinsii
1	HIERALCH	Hieronyma	alchorneoides
1	PACHAQUA	Pachira	aquatica
1	ORMOVELU	Ormosia	velutina
1	DUSSSPB	Dussia	sp. B
1	MELIOCCI	Meliosma	occidentalis
1	SWARNICA	Swartzia	nicaraguensis

1	SLOAMEDU	Sloanea	medusula
1	INGADENS	Inga	densiflora
1	COUEPOLY	Couepia	polyandra
1	STERRECO	Sterculia	recordiana
1	AMPEMACR	Ampelocera	macrocarpa
1	POUT1026	Pouteria	
2	PENTMACR	Pentaclethra	macroloba
2	TAPIGUIA	Tapirira	guianensis
2	GOETMEIA	Goethalsia	meiantha
2	VIROKOSC	Virola	koschnyi
2	VIROSEBI	Virola	sebifera
2	LAETPROC	Laetia	procera
2	APEIMEMB	Apeiba	membranacea
2	HERNDIDY	Hernandia	didymantha
2	POURBICO	Pourouma	bicolor
2	BALIELEG	Balizia	elegans
2	LECYAMPL	Lecythis	ampla
2	CASEARBO	Casearia	arborea
2	STRYMICR	Stryphnodendron	microstachyum
2	LACMPANA	Lacmellea	panamensis
2	BYRSARTH	Byrsonima	arthropoda
2	CORDBICO	Cordia	bicolor
2	INGALEIO	Inga	leiocalycina
2	GUATAERU	Guatteria	aeruginosa
2	OCOTHART	Ocotea	hartshorniana
2	PROTGLAB	Protium	glabrum
2	XYLOSERI	Xylopia	sericophylla
2	CALOBRAS	Calophyllum	brasiliense
2	HYMEMESO	Hymenolobium	mesoamericanum
2	CESPSPAT	Cespedesia	spathulata
2	VOUAANOM	Vouarana	anomala
2	TETRPANA	Tetragastris	panamensis
2	POURMINO	Pourouma	minor
2	ORMOOCHR	Ormosia	
2	INGASERT	Inga	sertulifera
2	ALCHFLOR	Alchorneopsis	floribunda
2	CONCPLEI	Conceveiba	pleiostemona
2	HAMPAPPE	Hampea	appendiculata
2	BAUHSP	Bauhinia	
2	PSEUSPUR	Pseudolmedia	spuria

2	POUT1019	Pouteria	
3	INGAPEZI	Inga	pezizifera
3	INGAALBA	Inga	alba
3	SIMAAMAR	Simarouba	amara
3	INGATHIB	Inga	thibaudiana
3	VOCHFERR	Vochysia	ferruginea
3	JACACOPA	Jacaranda	copaia
3	SPACCORR	Spachea	correae
3	VISMMACR	Vismia	macrophylla
4	WELFREGI	Welfia	regia
4	IRIADELT	Iriartea	deltoidea
4	GUARBULL	Guarea	bullata
4	PROTCONF	Protium	confusum
4	NAUCNAGA	Naucleopsis	naga
4	BROSLACT	Brosimum	lactescens
4	TRICSEPT	Trichilia	septentrionalis
4	CASSELLI	Cassipourea	elliptica
4	PINZCORI	Pinzona	coriacea
4	GUARRHOP	Guarea	rhopalocarpa
4	POUTTORT	Pouteria	torta
4	CUPAPSEU	Cupania	pseudostipularis
4	OCOTLAET	Ocotea	laetevirens
4	CASECOMM	Casearia	commersoniana
4	LICASARA	Licaria	sarapiquensis
4	SIPACUSP	Siparuna	cuspidata
4	ARDIFIMB	Ardisia	fimbrillifera
4	BOROPATI	Borojoa	patinoi
4	UNONPITT	Unonopsis	pittieri
4	CINNCHAV	Cinnamomum	chavarrianum
4	LICAARAC	Licania	arachicarpa
4	HEISCONC	Heisteria	concinna
4	RICHDRES	Richeria	dressleri
4	CHRYVENE	Chrysophyllum	venezuelanense
4	DALB1087	Dalbergia	
4	INGAACUM	Inga	acuminata
4	INGAPAVO		
4	PARAANTI		
4	CORDDWYE	Cordia	dwyeri
4	RHODKUNT	Rhodostemonodaphne	kunthiana
4	OCOTMACR	Ocotea	macropoda

4	BOROPANA	Borojoa	panamensis
4	COLUSPIN	Colubrina	spinosa
4	LACUPANA	Lacunaria	panamensis
4	NEEAELEG	Neea	elegans
4	THEOMAMM	Theobroma	mammosum
4	OCOTCERN	Ocotea	cernua
4	OCOTINSU	Ocotea	insularis
4	PRADLIND		
4	LICAMISA	Licaria	misantlae
4	POUTRETI	Pouteria	reticulata
4	SAPRVIRI	Sapranthus	viridiflorus
4	CECROBTU	Cecropia	obtusifolia
4	FARAGLAN	Faramea	glandulosa
4	POUT1023	Pouteria	
5	MICOMULT	Miconia	multispicata
5	INGAUMBE	Inga	umbellifera
5	SACOTRIC	Sacoglottis	trichogyna
5	SLOAGUIA	Sloanea	guianensis
5	MICOPUNC	Miconia	punctata
5	CHRYCOLO	Chrysophyllum	colombianum
6	SOCREXOR	Socratea	exorrhiza
6	CASTELAS	Castilla	elastica
6	EUTEPREC	Euterpe	precatoria
6	PRESPITT	Preslianthus	pittieri
6	RINODEFL	Rinorea	deflexiflora
6	ANAXCRAS	Anaxagorea	crassipetala
6	GUATAMPL	Guatteria	amplifolia
6	LIANSP		
6	COUSHOND	Coussarea	hondensis
6	DYSTPANI	Dystovomita	paniculata
6	HIRTLEMS	Hirtella	lemsii
6	PSYCPANA	Psychotria	panamensis
6	EUGESELV	Eugenia	selvana
6	ALCHLATI	Alchornea	latifolia
6	MICOSTEV	Miconia	stevensiana
6	PEREHISP	Perebea	hispidula
6	POSOPANA	Posoqueria	panamensis
6	ZYGIGIGA	Zygia	gigantifoliola
6	ANNOSUBN	Annona	subnubila
6	INGASP	Inga	

6	SWAROCHN	Swartzia	ochnacea
6	DRYPSTAN	Drypetes	standleyi
6	EUGESP	Eugenia	
6	GUARPILO	Guarea	pilosa
6	HANDCHRY	Handroanthus	chrysanthus
6	MELIDONN	Meliosma	donnellsmithii
6	QUIIMACR	Quiina	macrophylla
6	ARDISTAN	Ardisia	standleyana
6	EUGE945	Eugenia	
6	EUGEGLAN	Eugenia	glandulosopunctata
6	EUGELITH	Eugenia	lithosperma
6	JACADOLI	Jacaratia	dolichaula
6	LACIAGGR	Lacistema	aggregatum
6	MARILAXI	Marila	laxiflora
6	NECTCISS	Nectandra	cissiflora
6	NEEAAMPL	Neea	amplifolia
6	OCOTMOLL	Ocotea	mollifolia
6	ORMOINTE	Ormosia	intermedia
6	POUT981	Pouteria	
6	POUTDURL	Pouteria	durlandii
6	SYMPSTRI	Symplocos	striata
6	ASTRALAT	Astrocaryum	alatum
6	CASE-99	Casearia	
6	COUS9	Coussarea	
6	EUGEHART	Eugenia	hartshornii
6	LOZAPITT	Lozania	pittieri
6	MABEOCCI	Mabea	occidentalis
6	MAQUGUIA	Maquira	guianensis
6	MYRCALIE	Myrcia	aliena
6	PALICALI	Palicourea	calidicola
6	PARATRIC	Parathesis	trichogyne
6	PSYCLUXU	Psychotria	luxurians
6	BEILSP.A	Beilschmiedia	sp. A
6	POUT1004	Pouteria	
6	SLOAGENI	Sloanea	geniculata

References

1. Bohn, F.J., Frank, K. & Huth, A. (2014). Of climate and its resulting tree growth: Simulating the productivity of temperate forests. Ecological Modelling. 278. p.pp. 9–17.

2. Dantas de Paula, M., Groeneveld, J. & Huth, A. (2015). Tropical forest degradation and recovery in fragmented landscapes — Simulating changes in tree community, forest hydrology and carbon balance. Global Ecology and Conservation. 3. p.pp. 664–677.
3. Dislich, C., Günter, S., Homeier, J., Schröder, B. & Huth, A. (2009). Simulating forest dynamics of a tropical montane forest in South Ecuador. Erdkunde. 63 (4). p.pp. 347–364.
4. Dislich, C. & Huth, A. (2012). Modelling the impact of shallow landslides on forest structure in tropical montane forests. Ecological Modelling. 239. p.pp. 40–53.
5. Fischer, R., Bohn, F., Dantas de Paula, M., Dislich, C., Groeneveld, J., Gutiérrez, A.G., Kazmierczak, M., Knapp, N., Lehmann, S., Paulick, S., Pütz, S., Rödig, E., Taubert, F., Köhler, P. & Huth, A. (2016). Lessons learned from applying a forest gap model to understand ecosystem and carbon dynamics of complex tropical forests. Ecological Modelling. 326. p.pp. 124–133.
6. Fischer, R., Ensslin, A., Rutten, G., Fischer, M., Schellenberger Costa, D., Kleyer, M., Hemp, A., Paulick, S. & Huth, A. (2015). Simulating Carbon Stocks and Fluxes of an African Tropical Montane Forest with an Individual-Based Forest Model. Plos One. 10 (4). p.p. e0123300.
7. Groeneveld, J., Alves, L.F., Bernacci, L.C., Catharino, E.L.M., Knogge, C., Metzger, J.P., Pütz, S. & Huth, a. (2009). The impact of fragmentation and density regulation on forest succession in the Atlantic rain forest. Ecological Modelling. 220 (19). p.pp. 2450–2459.
8. Huth, A., Drechsler, M. & Köhler, P. (2004). Multicriteria evaluation of simulated logging scenarios in a tropical rain forest. Journal of environmental management. 71 (4). p.pp. 321–33.
9. Kammesheidt, L., Köhler, P. & Huth, A. (2001). Sustainable Timber Harvesting in Venezuela: A Modelling Approach. Journal of Applied Ecology. 38 (4). p.pp. 756–770.
10. Kazmierczak, M., Wiegand, T. & Huth, A. (2014). A neutral vs. non-neutral parametrizations of a physiological forest gap model. Ecological Modelling. 288. p.pp. 94–102.
11. Köhler, P. & Huth, A. (1998). The effects of tree species grouping in tropical rain forest modelling Simulations with the individual based model Formind. Ecological Modelling. 109 (3). p.pp. 301–321.
12. Pütz, S., Groeneveld, J., Henle, K., Knogge, C., Martensen, A.C., Metz, M., Metzger, J.P., Ribeiro, M.C., de Paula, M.D. & Huth, A. (2014). Long-term carbon loss in fragmented Neotropical forests. Nature communications. 5 (iDiv). p.p. 5037.
13. Shugart, H.H. (1984). A theory of forest dynamics: the ecological implications of forest succession models. New York, USA: Springer.
14. Sato, H., A. Itoh, and T. Kohyama, SEIB-DGVM: A new dynamic global vegetation model using a spatially explicit individual-based approach. Ecological Modelling, 2007. 200(3-4): p. 279-307.
15. Knapp N., Fischer R., Huth A.. Linking lidar and forest modeling to assess biomass estimation across scales and disturbance states. Remote Sensing of Environment (2018)
16. Bohlman & O’Brien (2006)
17. Brokaw (1985)

Appendix B: Model Calibration - Stem Number and Size Distribution

Parameters that could not be calculated or were not found in the CARBONO dataset were taken from an in-depth literature review. For example, maximum tree height by species was estimated from CARBONO data, Clark and Clark (1992, 2001), Dubayah et al. (2010), and King and Clark (2011). For canopy heights and aboveground biomass comparison, we referred to Dubayah et al. (2010) and Drake et al. (2002, 2003). Tree allometries, lifespans of some selected species and height classes were taken from King (1996). In addition, LAI was compared to Tang et al. (2012), and mean maximum photosynthetic rate (P_{max}) by shade tolerance class was compared to Oberbauer and Strain (1984). These comparisons were made to our calculations and to other forests in the region (Saatchi et al. 2011b; Chave et al. 2005, 2008, 2014; Clark and Clark 2000, 2001, 2006; Clark et al. 2008, 2015; Kellner et al. 2009; Hurtt et al. 2004). For example, in the case of the height-diameter relationship, factor form and biomass fraction allocation, the Knapp et al (2018) parameters from Barro Colorado Island (BCI) were used. BCI is a lowland rainforest of similar size to La Selva, with similar site demography and similar seasonal distribution of rainfall. There are numerous studies that compare measurements of flora or fauna from one site to the other (see: Freitas-Neto et al 2019; Shapiro and Pickering 2000; Bohlman and Pacala 2012; Beath 1999).

An important variable during model calibration, the resultant comparison of field measured to simulated stem numbers for all trees ≥10cm DBH are shown in Figure B-1, above. Over the course of the simulation, stem numbers follow the typical succession patterns described by Shugart (1984). After the initial high abundance of shade intolerant stems, shade intermediate and shade tolerant trees out-compete shade intolerant trees and dominate the canopy in an equilibrium state (*Figure B-1, (a)*). In comparing field observed stems to simulated stems, the model slightly underestimates total stem numbers, especially for shade intermediate large trees (PFT2) and shade tolerant small trees (PFT6) (*Figure B-1, (b)*). Analyzed by size class (*Figure B-1, (c)*), the model slightly overestimates smaller trees (<0.3m DBH), but slightly underestimates larger trees (0.4-0.5m).

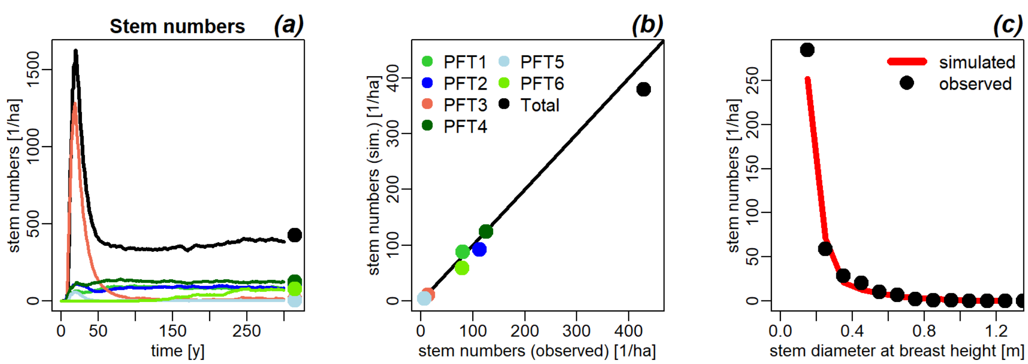

Figure B-1 (a) Time series showing stem numbers from bare ground at year 0 through simulation year 300 for all trees >10cm DBH. The dots at the far right show the stem numbers by PFT as calculated from the field data set. Dots correspond to PFT number and color groups are indicative of light requirements (i.e. greens are shade tolerant, blues shade intermediate, red shade intolerant and total in black). (b) The middle figure shows a one to one comparison of stem numbers between observed (field data) and simulated (FORMIND) by PFT. (c) The figure at right depicts stem numbers by diameter size class. Black dots are calculated from field data and the red line shows simulated values.

A further examination of the stem size distributions broken down by PFT is shown in Figure B-2. As shown by the figure, there is good agreement between each PFT for field measured and simulation produced trees, with a few exceptions. The simulation of PFT 1 trees slightly underestimates stem numbers of the smallest trees (0.10m – 0.20m), and the 0.50m-0.60m size class. For PFT 2 and PFT 3 there is slightly less agreement between simulated and observed stem numbers particularly for mid-sized trees. The PFT 2 observed stem numbers do not exhibit the typical J-curve size distribution patterning often observed in uneven-aged forests stands worldwide (Nyland 1998, Meyer 1952, DeLiocourt 1898). The smallest size classes were underestimated by the model for PFT 3, PFT 4, and PFT 6; whereas the PFT 1 overestimated the smallest size class stem numbers. The overall good agreement is indicative of the success of this FORMIND parameterization. The discrepancies are small (<20 stems per hectare) though could contribute slightly to error. Our calibration was aided by We performed a analysis by running the model hundreds of times, systematically changing certain parameters in small increments to achieve the best simulation of the study site forest (Lehmann and Huth 2015).

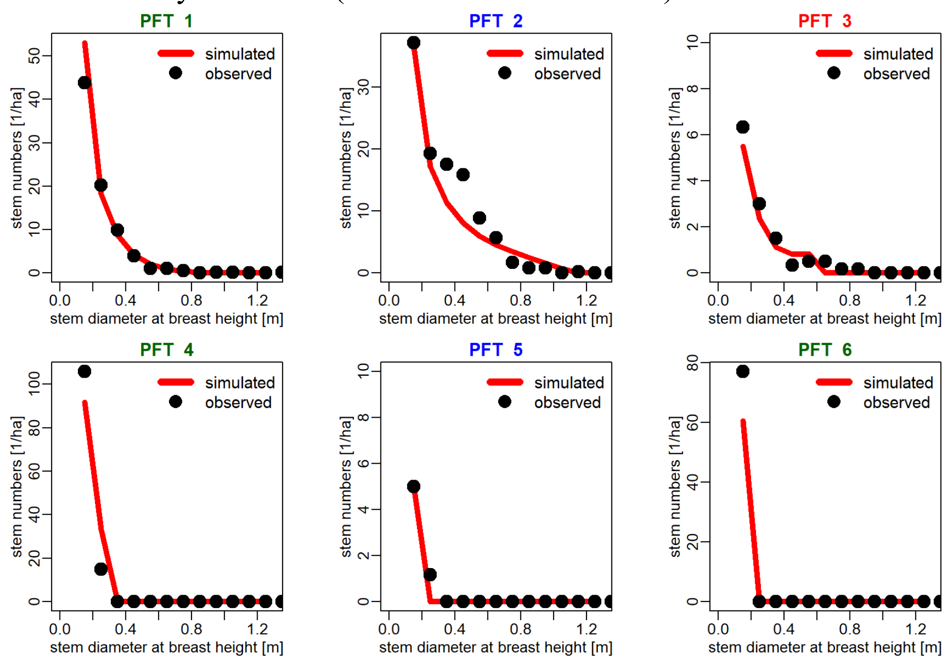

Figure B-2 Stem size distribution by PFT, beginning with PFT1 in the upper left, to PFT6 in the lower right. The observed (black dots) values were calculated from the field dataset. The red line plots values obtained from the FORMIND simulation. The label color for the PFTs corresponds to light requirements, such that green is shade tolerant, blue is shade intermediate and red is shade intolerant.

With respect to tree height, Figure B-3 indicates that the forest height (m) as simulated by the FORMIND model compares well with Kellner et al.'s 2009 study. Mean forest height, or the average of the Lorey's height for each 10m pixel, as shown in Figure B-3 (at right) has a slightly larger overall range, but with very similar mid-points (black dots). The forest has the spatial configuration of a mixed age rainforest stand (B-3, left), with heights ranging from canopy emergent trees, nearly 50m tall, to the canopy gaps consisting of holes with regeneration less than 10m in height. A frequency analysis of tree height distribution of the simulated study forest indicates underestimates the frequency of 10m and 20m trees, and overestimates 14m and 16m trees. However, the overall average forest height matches that of Kellner (2009).

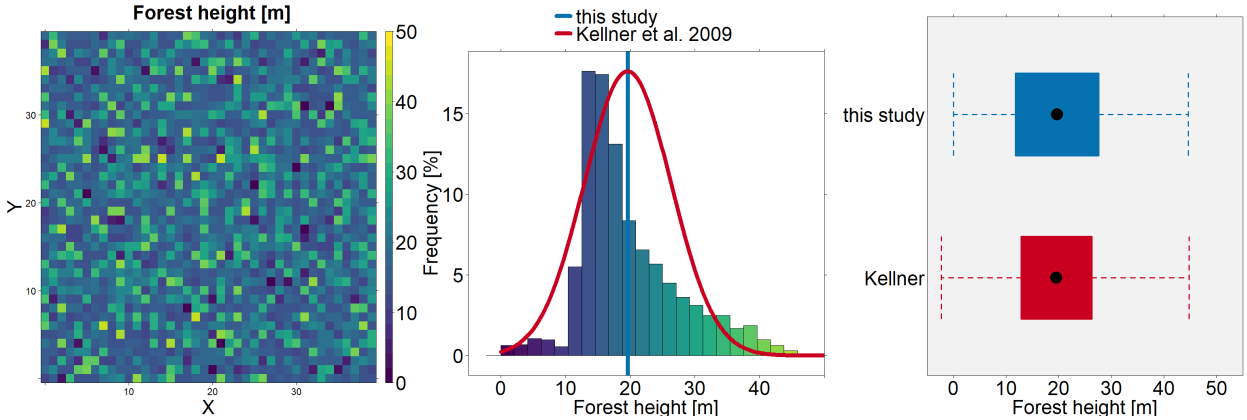

Figure B-3 The forest height of the simulated forest is compared with Kellner et al 2009's findings. *At left*: a sample of simulated forest is shown with heights given by colors from 0m to 50m (scale at the right). Here, forest height is defined as Lorey's height at 10m pixel resolution. *At center:* A frequency distribution of forest heights (i.e., Lorey's height) is given as compared to Kellner et al 2009. Blue line indicates the average forest height of our study. *At right:* Kellner et al 2009 range of forest height values is compared to those simulated by the FORMIND model in this study as box-and-whisker plots.

References

1. Beath, D.N., 1999. Dynastine scarab beetle pollination in Dieffenbachia longispatha (Araceae) on Barro Colorado Island (Panama) compared with La Selva biological station (Costa Rica). Aroideana, 22, pp.63-71.
2. Bohlman, S. and Pacala, S., 2012. A forest structure model that determines crown layers and partitions growth and mortality rates for landscape-scale applications of tropical forests. Journal of Ecology, 100(2), pp.508-518.
3. Chave, J., Andalo, C., Brown, S., Cairns, M.A., Chambers, J.Q., Eamus, D., Fölster, H., Fromard, F., Higuchi, N., Kira, T. and Lescure, J.P., 2005. Tree allometry and improved estimation of carbon stocks and balance in tropical forests. Oecologia, 145(1), pp.87-99.
4. Chave, J., Olivier, J., Bongers, F., Châtelet, P., Forget, P.M., van der Meer, P., Norden, N., Riéra, B. and Charles-Dominique, P., 2008. Above-ground biomass and productivity in a rain forest of eastern South America. Journal of Tropical Ecology, 24(4), pp.355-366.
5. Chave, J., Réjou-Méchain, M., Búrquez, A., Chidumayo, E., Colgan, M.S., Delitti, W.B., Duque, A., Eid, T., Fearnside, P.M., Goodman, R.C. and Henry, M., 2014. Improved allometric models to estimate the aboveground biomass of tropical trees. Global change biology, 20(10), pp.3177-3190.
6. Clark, D.A. and Clark, D.B., 1992. Life history diversity of canopy and emergent trees in a neotropical rain forest. Ecological monographs, 62(3), pp.315-344.
7. Clark, D.B. and Clark, D.A., 2000. Landscape-scale variation in forest structure and biomass in a tropical rain forest. Forest ecology and management, 137(1), pp.185-198.
8. Clark, D.A. and Clark, D.B., 2001. Getting to the canopy: tree height growth in a neotropical rain forest. Ecology, 82(5), pp.1460-1472.

9. Clark, D. B., and D. A. Clark. 2006. Tree growth, mortality, physical and microsite in an old-growth lowland tropical rain forest. Ecology, 87, 2132, http://www.esapu bs.org /arc hive/e col/E087/132de fault.htm.
10. Clark, D.B., Olivas, P.C., Oberbauer, S.F., Clark, D.A. and Ryan, M.G., 2008. First direct landscape-scale measurement of tropical rain forest Leaf Area Index, a key driver of global primary productivity. Ecology letters, 11(2), pp.163-172.
11. Clark, D.A., Clark, D.B. and Oberbauer, S.F., 2013. Field-quantified responses of tropical rainforest aboveground productivity to increasing CO2 and climatic stress, 1997–2009. Journal of Geophysical Research: Biogeosciences, 118(2), pp.783-794.
12. DeLiocourt, F. 1898. De l'amenagement des Sapinieres. Bulletin De la Societe Forestiere de Franch-Conte et Belfort.
13. Drake, J.B., Dubayah, R.O., Clark, D.B., Knox, R.G., Blair, J.B., Hofton, M.A., Chazdon, R.L., Weishampel, J.F. and Prince, S., 2002. Estimation of tropical forest structural characteristics using large-footprint lidar. Remote Sensing of Environment, 79(2), pp.305-319.
14. Drake, J.B., Knox, R.G., Dubayah, R.O., Clark, D.B., Condit, R., Blair, J.B. and Hofton, M., 2003. Above-ground biomass estimation in closed canopy neotropical forests using lidar remote sensing: Factors affecting the generality of relationships. Global ecology and biogeography, 12(2), pp.147-159.
15. Dubayah, R.O., Sheldon, S.L., Clark, D.B., Hofton, M.A., Blair, J.B., Hurtt, G.C. and Chazdon, R.L., 2010. Estimation of tropical forest height and biomass dynamics using lidar remote sensing at La Selva, Costa Rica. Journal of Geophysical Research: Biogeosciences, 115(G2).
16. Freitas-Neto, J.F., Sousa, J.O., Ovrebo, C.L. and Baseia, I.G, 2019. Geastrum echinulatum and G. rusticum (Geastraceae, Basidiomycota)–two new records for Central America.
17. Hurtt, G.C., Dubayah, R., Drake, J., Moorcroft, P.R., Pacala, S. and Fearon, M., 2004. Beyond potential vegetation: combining lidar remote sensing and a height-structured ecosystem model for improved estimates of carbon stocks and fluxes. Ecological Applications, 14(3), pp.873-883.
18. Kellner, J.R., Clark, D.B. and Hubbell, S.P., 2009. Pervasive canopy dynamics produce short-term stability in a tropical rain forest landscape. Ecology Letters, 12(2), pp.155-164.
19. King, D.A., 1996. Allometry and life history of tropical trees. Journal of tropical ecology, 12(1), pp.25-44.
20. King, D.A. and Clark, D.A., 2011. Allometry of emergent tree species from saplings to above-canopy adults in a Costa Rican rain forest. Journal of Tropical Ecology, 27(6), pp.573-579.
21. Lehmann, S. and Huth, A., 2015. Fast calibration of a dynamic vegetation model with minimum observation data. Ecological modelling, 301, pp.98-105.
22. Meyer, H. A. 1952. Structure, growth, and drain in balanced, uneven-aged forests. Journal of Forestry. 52: 85-92.
23. Nyland, R. D. 1998. Selection system in northern hardwoods. Journal of Forestry. 96: 18-21. Remote Sensing of Environment, 124, pp.242-250.Oberbauer and Strain 1984
24. Saatchi, S., Marlier, M., Chazdon, R.L., Clark, D.B. and Russell, A.E., 2011b. Impact of spatial variability of tropical forest structure on radar estimation of aboveground biomass. Remote Sensing of Environment, 115(11), pp.2836-2849.
25. Shapiro, B.A. and Pickering, J., 2000. Rainfall and parasitic wasp (Hymenoptera: Ichneumonoidea) activity in successional forest stages at Barro Colorado Nature Monument,

Panama, and La Selva Biological Station, Costa Rica. Agricultural and Forest Entomology, 2(1), pp.39-47.

26. Shugart, H.H., 1984. A theory of forest dynamics. The ecological implications of forest succession models. Springer-Verlag.
27. Tang, H., Dubayah, R., Swatantran, A., Hofton, M., Sheldon, S., Clark, D.B. and Blair, B., 2012. Retrieval of vertical LAI profiles over tropical rain forests using waveform lidar at La Selva, Costa Rica

Appendix C: Aboveground biomass comparison to height metrics

Though the primary goal of this research was to investigate how the accuracy of the correlation of height to AGB, LAI and GPP changes if analyzed on different spatial scales, it is also important to consider how the correlation changes depending on the height metric used. Lorey's Height was the height metric analyzed and presented in the main text body of this manuscript, however we also analyzed the correlation of aboveground biomass to RH100, mean height and canopy height at the four plot sizes (10m, 20, 50m, 100m). Following the same methodology as with the Lorey's Height comparison, 8000 data points were collected for each plot size so as not to introduce artificial bias into the dataset with an uneven number of points for the analysis. In this section we will present the analysis of RH100, canopy height and mean height.

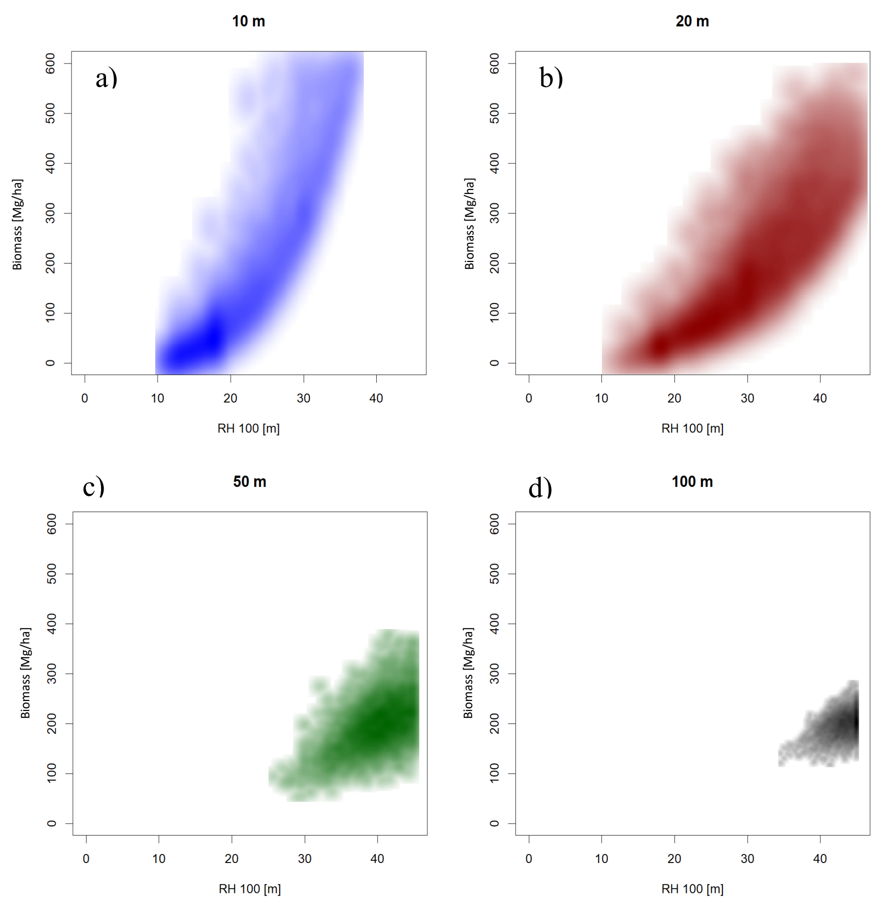

Figure C-1 The four plots display the relationship between RH100 (m) and aboveground biomass (Mg_{odm}/ha) at plot scales of (a) 10x10m ($100m^2$ = 0.01ha) in blue, (b) 20x20m ($400m^2$ = 0.04ha) in red, (c) 50x50m ($2500m^2$ = 0.25ha) in green, and (d) 100x100m ($10000m^2$ = 1.0ha) in black. Note: For the purposes of visual comparison, the scale of figures (a) through (d) was kept consistent. The datasets in the figures are not truncated.

AGB was also compared to RH100 (Figure C-1), canopy height (Figure C-2) and mean height (Figure C-3), at the 10m, 20m, 50m and 100m plot sizes. At 10m resolution, RH100 predicted AGB with the highest R^2 fit relationship of all the height metrics at all plot resolutions. In comparing the point clouds at each plot resolution, the 10m and 20m plot resolutions resemble a power law relationship (Figure C-1 a and b, respectively), whereas the 50m and 100m point clouds only extend along part of a power curve (Figure C-1 c and d, respectively), with the size of the point cloud decreasing from higher to lower resolution. Overall, the most complete power curve with the densest cloud over the full curve is at the 10m resolution.

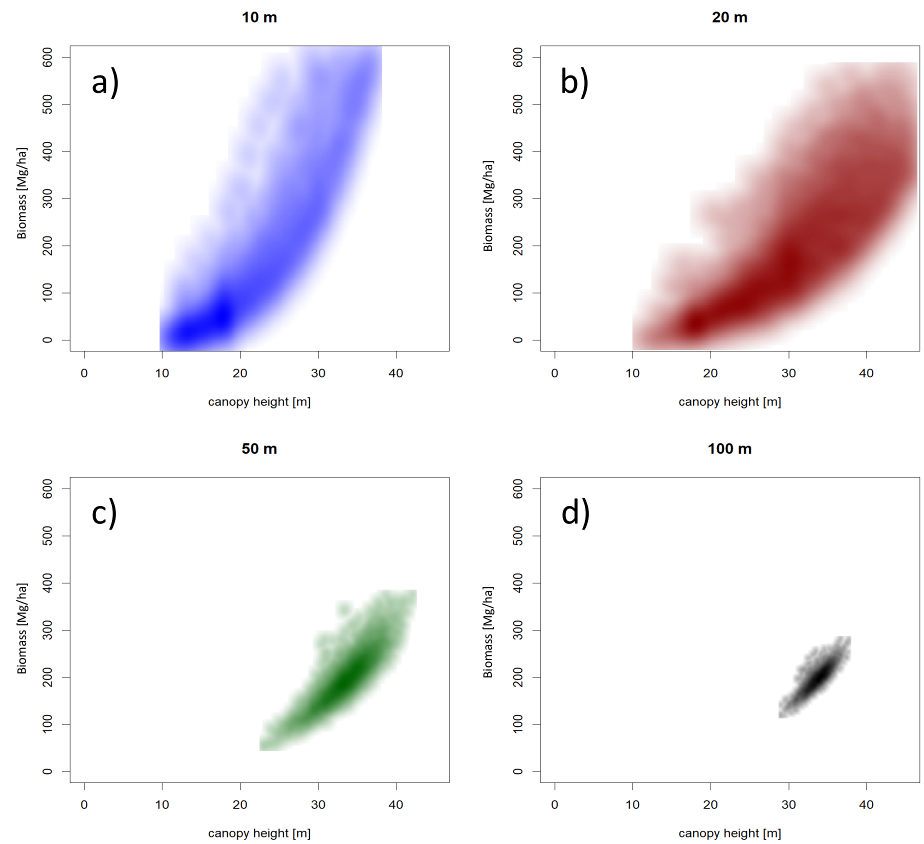

Figure C-2 The four plots display the relationship between canopy height (m) and aboveground biomass (Mg_{odm}/ha) at plot scales of (a) 10x10m ($100m^2 = 0.01$ha) in blue, (b) 20x20m ($400m^2 = 0.04$ha) in red, (c) 50x50m ($2500m^2 = 0.25$ha) in green, and (d) 100x100m ($10000m^2 = 1.0$ha) in black. Note: For the purposes of visual comparison, the scale of figures (a) through (d) was kept consistent. The datasets in figures are not truncated.

The canopy height used in this study is the same measure used in Kohler and Huth's 2010 study on ground-truthing spaceborne estimates of above-ground biomass in tropical rain forests in Sabah, Malaysia. Similar to RH100, the curves all represent the relationship as a power law function (see Figure C-2). Point clouds at the 50m and 100m resolutions (Figure C-2 c and d, respectively) have decreasingly smaller and more concentrated shapes, only covering a small area of the representative relationship curve. The point cloud shape at 100m is so small that the relationship cannot be not clearly defined as a power law curve (or any other type). In comparing 10m to 20m resolutions (Figure C-2 a and b), both point clouds range over the entire curve equation range. The 20m resolution relationship point cloud appears to be more diffuse than the 10m resolution.

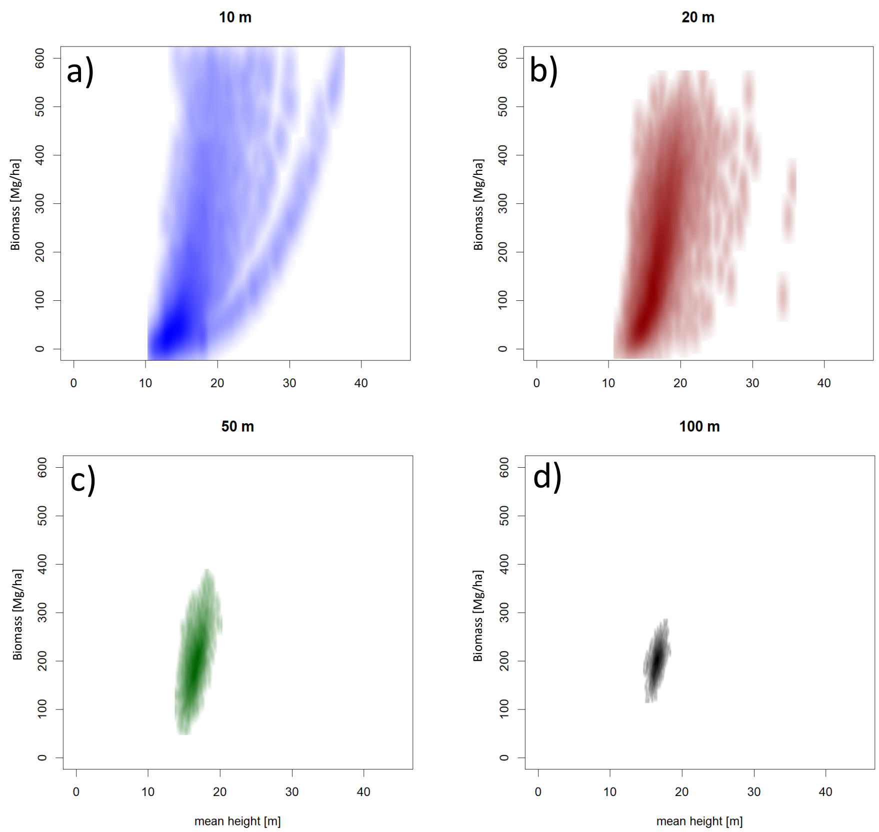

Figure C-3 The four plots display the relationship between mean height (m) and aboveground biomass (Mg_{odm}/ha) at plot scales of (a) 10x10m ($100m^2 = 0.01$ha) in blue, (b) 20x20m ($400m^2 = 0.04$ha) in red, (c) 50x50m ($2500m^2 = 0.25$ha) in green, and (d) 100x100m ($10000m^2 = 1.0$ha) in black. Note: For the purposes of visual comparison, the scale of figures (a) through (d) was kept consistent. However, the datasets in figures are not truncated.

In addition, mean canopy height was also plotted against aboveground biomass for the four resolutions of interest in this study (Figure C-3). At each resolution, the relationship was comparatively weaker than that of each of the other height metrics investigated in this study. Though a power law curve was also the best type of equation to explain the plotted relationship, the fit of the data to this curve shape is poor at best (Figure C-3, a and b) and barely recognizable at low resolutions (Figure C-3, c and d). The shape of the data points for the 100m plot resolution (Figure C-3, d) is almost vertical and linear, with points highly concentrated over a small range of heights. At the 50m resolution (Figure C-3, c), the relationship is very similar to that of the 100m plot resolution, however the almost vertical line shaped point cloud is slightly less concentrated, indicating and increased range in the value of the data points. In contrast, the 10m and 20m plot resolutions (Figure C-3, a and b, respectively) have a larger range of points, with a more clearly defined power law relationship shape. However, the point clouds at both plot resolutions appear to be more diffuse, with in increased number of outlier points, as compared to the other height metric correlations.

As shown in Figure C-4 below, the comparison of r^2 and RMSE for all plot resolutions indicates that there is a tradeoff between accuracy and precision within this dataset. For instance, canopy height has the highest level of accuracy, with r^2 values from 0.91 for the 10m resolution plots to 0.77 for the 100m plots. However, the RMSE ranges from 82.5 to 12.0 from 10m to 100m, respectively. In addition, there is little difference in r^2 values from 20m (0.80) to 50m (0.81), but a substantial improvement in RMSE: from 62.9 to 40.2, for the 20m and 50m. If using canopy height as a chosen metric, 50m resolution plots are more advantageous than 20m plots, and the decrease in error may be worth the accuracy lost (see figure C-4). The RH100 height metric had a rapid decrease in both accuracy and precision with increasing plot size. While the RMSE was lowest (21.5) at 100m plot resolution, the r^2 value was 0.14, highlighting the lack of relationship when relating RH100 to aboveground biomass at courser scales. As shown in Figure C-4 in the bottom left figure, the r^2 and RMSE are tightly coupled in terms of their downward trend. The largest drop in RMSE (>25%) from 10m to 20m, but the r^2 decreases to 0.80. Thus, at 20m, roughly the size of a single tree canopy in a tropical forest if viewed from the top down, there is a greater balance in accuracy and precision. The mean canopy height exhibited the weakest overall relationship with aboveground biomass, with the highest RMSE at the 10m and 20m plot resolutions (Figure C-4, bottom right). Though the same decreasing trends of r^2 and RMSE with increasing plot sizes was evident, the small r^2 values suggest an overall weak relationship that should not be considered for analysis.

	R^2 (Power Law)				***RMSE (Power Law)***			
Plot Resolution	***Lorey's Height***	**RH100**	**Canopy Height**	**Mean Height**	***Lorey's Height***	**RH100**	**Canopy Height**	**Mean Height**
10m	*0.83*	0.91	0.91	0.61	*130.5*	84.7	82.5	461.3
20m	*0.70*	0.80	0.80	0.43	*76.3*	62.9	63.0	113.3
50m	*0.60*	0.32	0.81	0.35	*31.3*	40.2	22.3	37.9
100m	*0.53*	0.14	0.77	0.30	*16.0*	21.5	12.0	19.2

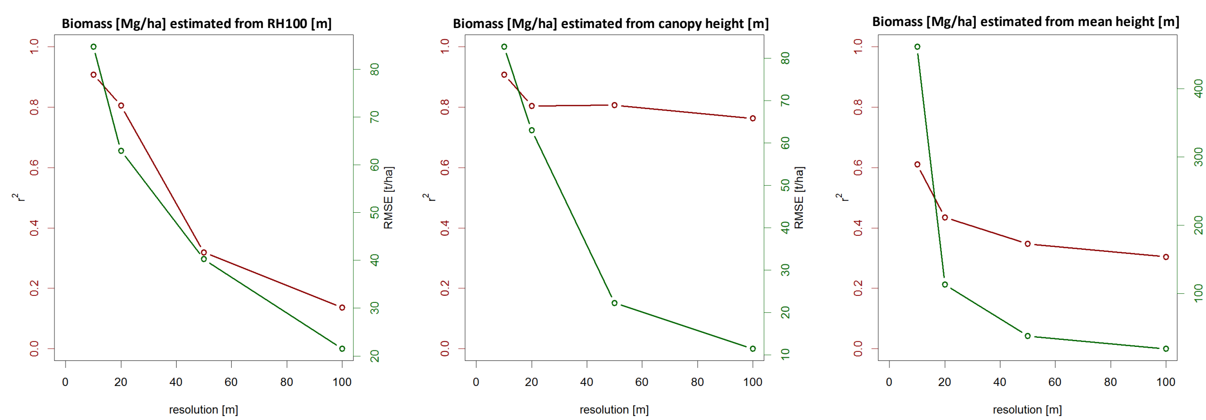

Figure C-4 *The table at the top shows numeric values for r^2 and root mean squared error (RMSE) for each of the height definitions at each plot resolution. The graphs at the bottom show the inverse relationship between r^2 and RMSE values. In all three graphs, plot resolution is on the x-axis, r^2 is and RMSE are on the primary (red) and secondary y-axis (green), respectively. At left: Biomass estimated from RH100 (m). At middle: Biomass estimated from canopy height (m). At right: Biomass estimated from mean height (m).*

References

Köhler, P. and Huth, A., 2010. Towards ground-truthing of spaceborne estimates of above-ground life biomass and leaf area index in tropical rain forests. *Biogeosciences*, *7*, pp.2531-2543.

Appendix D Leaf Area Index comparison to height metrics

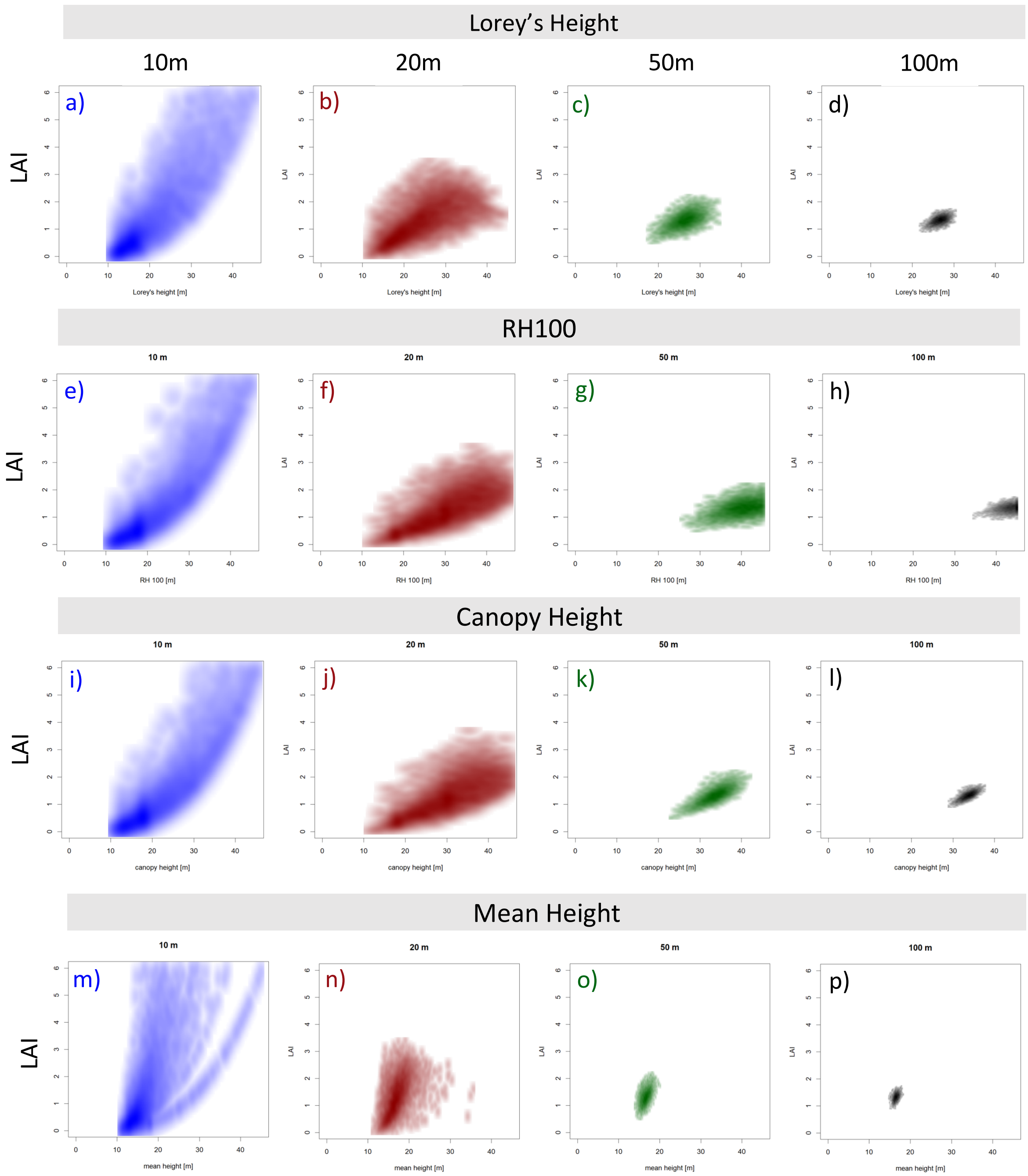

Figure D-1 *The matrix of plots presents the correlation of height to LAI at four plot scales and for each of the four height metrics analyzed in this study. The four spatial scales are color coded as the following: 10m in blue (plots a, e, i and m), 20m in red (plots b, f, j and n), 50m in green (plots c, g, k and o), and 100m in black (plots d, h, l and p). The four height metrics correlated consist of: Lorey's Height (plots a through d), RH100 (plots e through h), Canopy Height (plots i through l), and Mean Height (plots m through p).*

FORMIND successfully characterizes total tree LAI amongst the trees included in the simulation (trees >10cm DBH) if comparing with the results presented in Tang et al (2012) and Clark et al (2008). A well-known driver of productivity, LAI is typically measured at plot or even individual tree scales. However, in relating LAI to height metrics, extrapolation from plot to landscape scale could provide new information about forest productivity, with the potential to be quantified through time using remotely sensed datasets. The success of this approach hinges the ability of height to predict LAI within a study forest.

Our correlation comparisons of the height metrics to LAI overall indicates that there is good relatability in La Selva study forest, though the accuracy and precision of the relationship depends on the scale and height metric used. As shown in Figure D-1, at 10m plot resolution RH100, canopy height and to a slightly lesser degree Lorey's Height, have a clearly defined relationship over the full range of height values found in the forest. The 10m and 20m resolution correlations for all four height metrics compared relate to LAI best with power law equations, though the exponent would be smaller in the 20m equations, based on the point concentrations. The 50m and 100m plots decreasing point spread size, thus the equation does not relate over the entire range of height values. Mean height was not an appropriate height metric for predicting LAI at any resolution. Visually, the canopy height and RH100 relationships appear to be nearly identical at the 10m and 20m resolution but diverge at 50m and 100m. At 50m and 100m, the canopy height/LAI relationship more closely resembles that of Lorey's Height.

	R^2 (Power Law)				***RMSE (Power Law)***			
Plot Resolution	**Lorey's Height**	**RH100**	**Canopy Height**	**Mean Height**	**Lorey's Height**	**RH100**	**Canopy Height**	**Mean Height**
10m	*0.75*	0.84	0.84	0.54	*0.7*	0.6	0.6	1.6
20m	*0.51*	0.66	0.65	0.33	*0.5*	0.4	0.4	0.6
50m	*0.35*	0.19	0.62	0.25	*0.2*	0.2	0.2	0.2
100m	*0.27*	0.08	0.55	0.20	*0.1*	0.1	<0.1	0.1

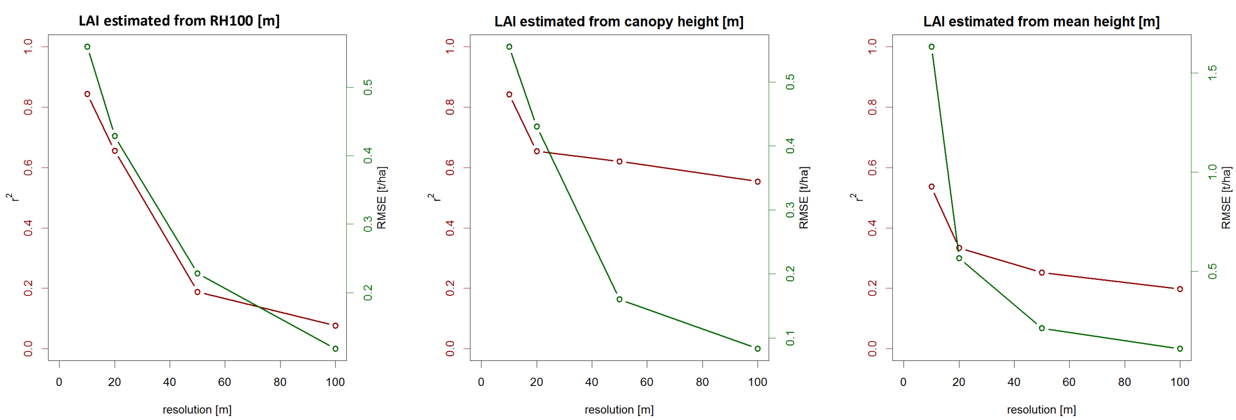

Figure D-1 *The table at the top shows numeric values for R^2 and root mean squared error (RMSE) for each of the height definitions correlated with LAI at each plot resolution. The graphs at the bottom show the inverse relationship between R^2 and RMSE values. In all three graphs, plot resolution is on the x-axis, R^2 is and RMSE are on the primary (red) and secondary y-axis (green), respectively. At left: LAI estimated from RH100 (m). At middle: LAI estimated from canopy height (m). At right: LAI estimated from mean height (m).*

As with the AGB/height correlations, across all definitions there exists a trade-off between accuracy (R^2) and precision (RMSE) across the 4 spatial scales. R^2 values are the highest for RH100 and canopy height (Figure D-2), however RMSE is also comparatively high. Conversely, RMSE is lowest for all height definitions at 100m when R^2 values are the lowest. Though the height/LAI correlation is very similar at the 20m resolution for RH100 and canopy height, they differ dramatically at 50m resolution. For RH100, the correlation is no longer present at 50m resolution and the R^2 decreases by 0.47, whereas the strength of the canopy height correlation at from 20m to 50m resolution only decreases by 0.03. For both height metrics, the RMSE is reduced by half, however. It therefore becomes apparent that the choice of height metric is as important as considering the scale in using height to predict LAI.

References

Clark, D.B., Olivas, P.C., Oberbauer, S.F., Clark, D.A. and Ryan, M.G., 2008. First direct landscape-scale measurement of tropical rain forest Leaf Area Index, a key driver of global primary productivity. *Ecology letters*, *11*(2), pp.163-172.

Tang, H., Dubayah, R., Swatantran, A., Hofton, M., Sheldon, S., Clark, D.B. and Blair, B., 2012. Retrieval of vertical LAI profiles over tropical rain forests using waveform lidar at La Selva, Costa Rica. Remote Sensing of Environment, 124, pp.242-250.

Appendix E Relating GPP to height metrics

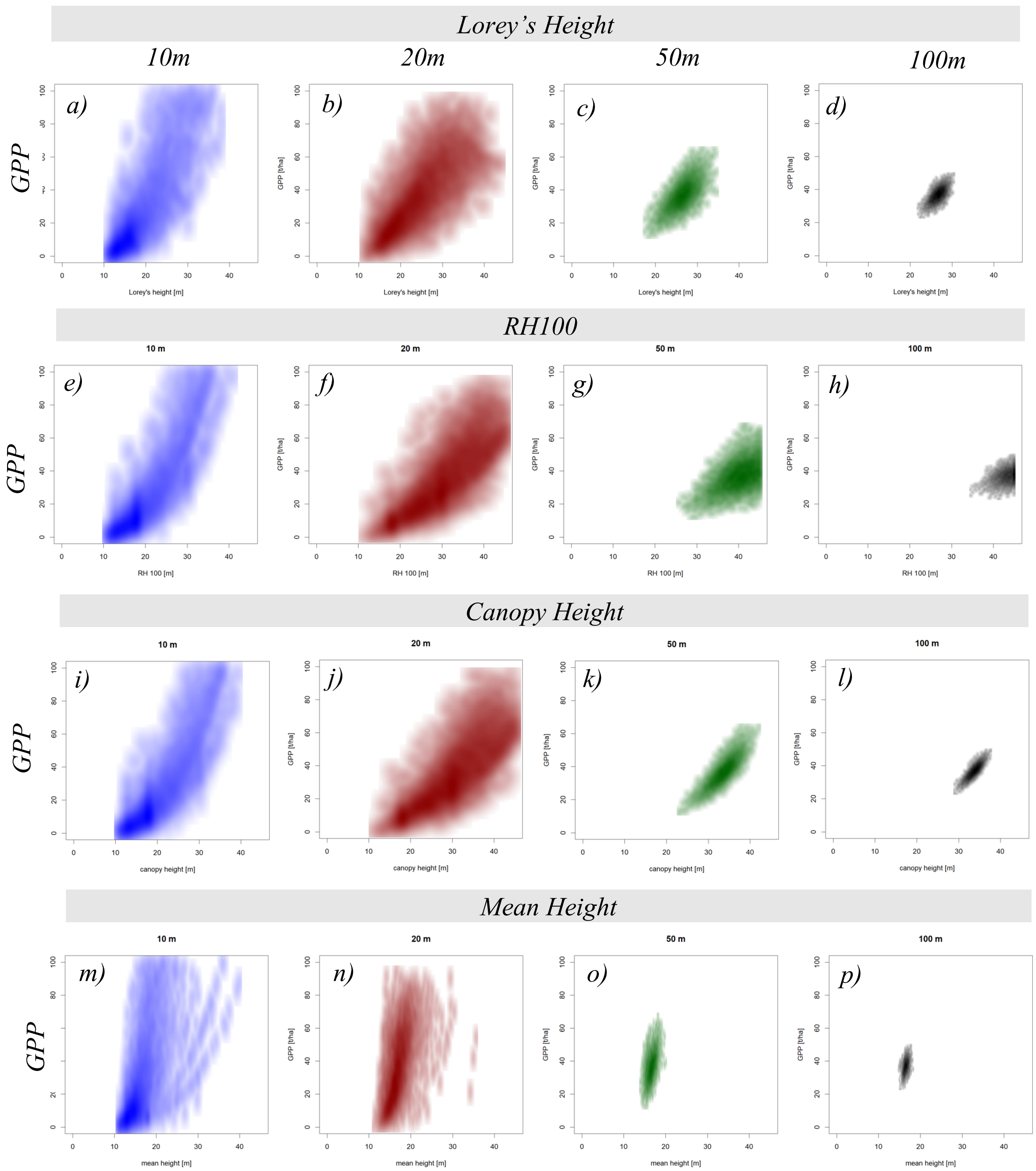

Figure E-1 *The matrix of plots presents the correlation of height to GPP at four plot scales and for each of the four height metrics analyzed in this study. The four spatial scales are color coded as the following: 10m in blue (plots a, e, i and m), 20m in red (plots b, f, j and n), 50m in green (plots c, g, k and o), and 100m in black (plots d, h, l and p). The four height metrics correlated consist of: Lorey's Height (plots a through d), RH100 (plots e through h), Canopy Height (plots i through l), and Mean Height (plots m through p). Note: For the purposes of visual comparison, the scale of all plots was kept consistent. However, the dataset presented in each plot is not truncated.*

The highest GPP per unit area worldwide is found in tropical rainforests like that of our study site; tropical forests account for 34% of the global terrestrial GPP (Beer et al., 2010). Though GPP typically refers to a carbon flux at the ecosystem level rather than on an individual tree level, respiration and growth are individual functions that are scaled up to be relatable to GPP, and in the case of respiration, subtracted from GPP to calculate net primary production (NPP) (Propastin et al 2012). Plant respiration has been shown to be proportional to, or a relatively stable fraction of GPP (Propastin et al 2012; Waring et al., 1998; Gifford, 2003). The measure of leaf area exhibits the strongest biotic control on GPP (Yang et al., 2016; Gower et al., 200; Duursma et al., 2009), and as shown in the previous section, leaf area correlates strongly with tree height.

We therefore investigated correlating GPP with tree height from 10m to 100m resolution (Figure E-1) and found a similar trade-off between accuracy and precision that was seen in other variables (Appendx C and D). A visual comparison of the results matrix in Figure E-1 highlights the similarities of RH100 and canopy height at 10m and 20m resolution though the behavior of the datasets diverges at 50m and 100m resolution. As with the other variables tested, the finer resolution plots indicate that height relates best to GPP using a power law relationship. At the 10m and 20m resolutions, points concentrate along where the equation line would be located, and the points extend across the full range of heights. The 50m and 100m resolutions not clearly related by a power law, and appear as all 8000 points concentrated at the larger end of the height range. Mean canopy height exhibited the weakest correlation at all scales, ranging from 0.56 at 10m resolution to 0.19 at 100m resolution (Figure E-2). At the coarser resolutions, Lorey's Height more closely resembles canopy height, whereas RH100 height saturates.

	R^2 (Power Law)				***RMSE (Power Law)***			
Plot Resolution	**Lorey's Height**	**RH100**	**Canopy Height**	**Mean Height**	**Lorey's Height**	**RH100**	**Canopy Height**	**Mean Height**
10m	*0.78*	0.86	0.99	0.56	*21.6*	15.5	15.5	61.1
20m	*0.61*	0.73	0.72	0.37	*13.3*	11.4	11.5	17.5
50m	*0.50*	0.28	0.75	0.26	*5.7*	6.8	4.1	6.7
100m	*0.43*	0.10	0.73	0.19	*2.9*	3.6	2.0	3.4

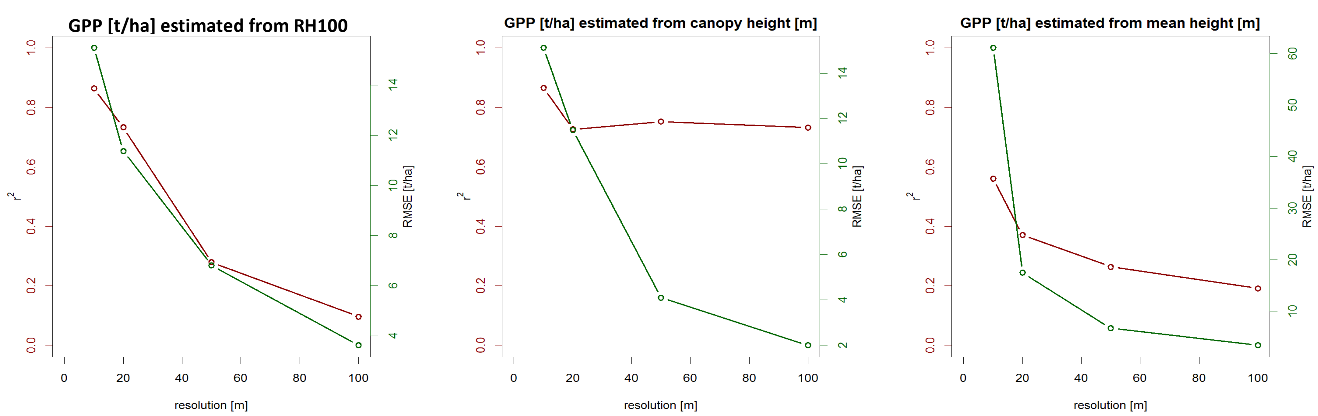

Figure E-2 *The table at the top shows numeric values for R^2 and root mean squared error (RMSE) for each of the height definitions correlated with GPP at each plot resolution. The graphs at the bottom show the inverse relationship between R^2 and RMSE values. In all three graphs, plot resolution is on the x-axis, R^2 is and RMSE are on the primary (red) and secondary y-axis (green), respectively. At left: GPP estimated from RH100 (m). At middle: GPP estimated from canopy height (m). At right: GPP estimated from mean height (m).*

Canopy height and RH100 had the overall strongest correlations with GPP, with the highest R^2 values of 0.99 and 0.86 respectively at 10m resolution. The accuracy and precision trade-offs were markedly different for each of the height metrics investigated (Figure E-2). Whereas the RMSE and R^2 decreased proportionally from 10m (R^2: 0.86; RMSE: 15.5) to 100m (R^2: 0.10; RMSE: 3.6) resolution in the RH100/GPP comparison, the decrease in R^2 was comparatively less (10m: 0.99;100m: 0.73) in the canopy height correlation, though the decrease in RMSE was very similar to that of RH100. These results suggest that for correlating height with GPP, the height definition used is arguably as important as the resolution considered.

References

Beer, C., Reichstein, M., Tomelleri, E., Ciais, P., Jung, M., Carvalhais, N., Rödenbeck, C., Arain, M.A., Baldocchi, D., Bonan, G.B. and Bondeau, A., 2010. Terrestrial gross carbon dioxide uptake: global distribution and covariation with climate. *Science*, *329*(5993), pp.834-838.

Duursma, R.A., Kolari, P., Perämäki, M., Pulkkinen, M., Mäkelä, A., Nikinmaa, E., Hari, P., Aurela, M., Berbigier, P., Bernhofer, C. and Grünwald, T., 2009. Contributions of climate, leaf area index and leaf physiology to variation in gross primary production of six coniferous forests across Europe: a model-based analysis. *Tree physiology*, *29*(5), pp.621-639.

Gifford, R.M., 2003. Plant respiration in productivity models: conceptualisation, representation and issues for global terrestrial carbon-cycle research. *Functional Plant Biology*, *30*(2), pp.171-186.

Gower, S.T., Krankina, O., Olson, R.J., Apps, M., Linder, S. and Wang, C., 2001. Net primary production and carbon allocation patterns of boreal forest ecosystems. *Ecological applications*, *11*(5), pp.1395-1411.

Propastin, P., Ibrom, A., Knohl, A. and Erasmi, S., 2012. Effects of canopy photosynthesis saturation on the estimation of gross primary productivity from MODIS data in a tropical forest. Remote Sensing of Environment, 121, pp.252-260.

Waring, R.H., Landsberg, J.J. and Williams, M., 1998. Net primary production of forests: a constant fraction of gross primary production? *Tree physiology*, *18*(2), pp.129-134.

Yang, J., He, Y., Aubrey, D.P., Zhuang, Q. and Teskey, R.O., 2016. Global patterns and predictors of stem CO 2 efflux in forest ecosystems. *Global change biology*, *22*(4), pp.1433-1444.

Appendix F: Relationship between R^2 and RMSE

The relationships between R^2 and nRMSE from the correlations of AGB, LAI and GPP with the height metrics across the different scales are shown in Figure F-1. The objective of a high R^2 and a low nRMSE would result in points concentrating in the lower right quadrant of the plot space. As shown in F-1 a through d, though no height definition had correlations that resulted in high R^2 and low nRMSE, canopy height and the 10m and 20m resolution RH100 correlations were the closest to the lower right quadrant. Canopy height, RH100, and mean height had similar relationships across the variables tested (AGB, LAI and GPP); the Lorey's height correlations differed slightly between the tested variables such that the AGB line had the largest slope, indicating that the R^2 decreased the least while nRMSE decreased the most between 10m and 100m resolution, of the three variables tested. Conversely, the LAI relationship with Lorey's height went from meaningful to not meaningful in comparing R^2 values from 10m to 100m resolution.

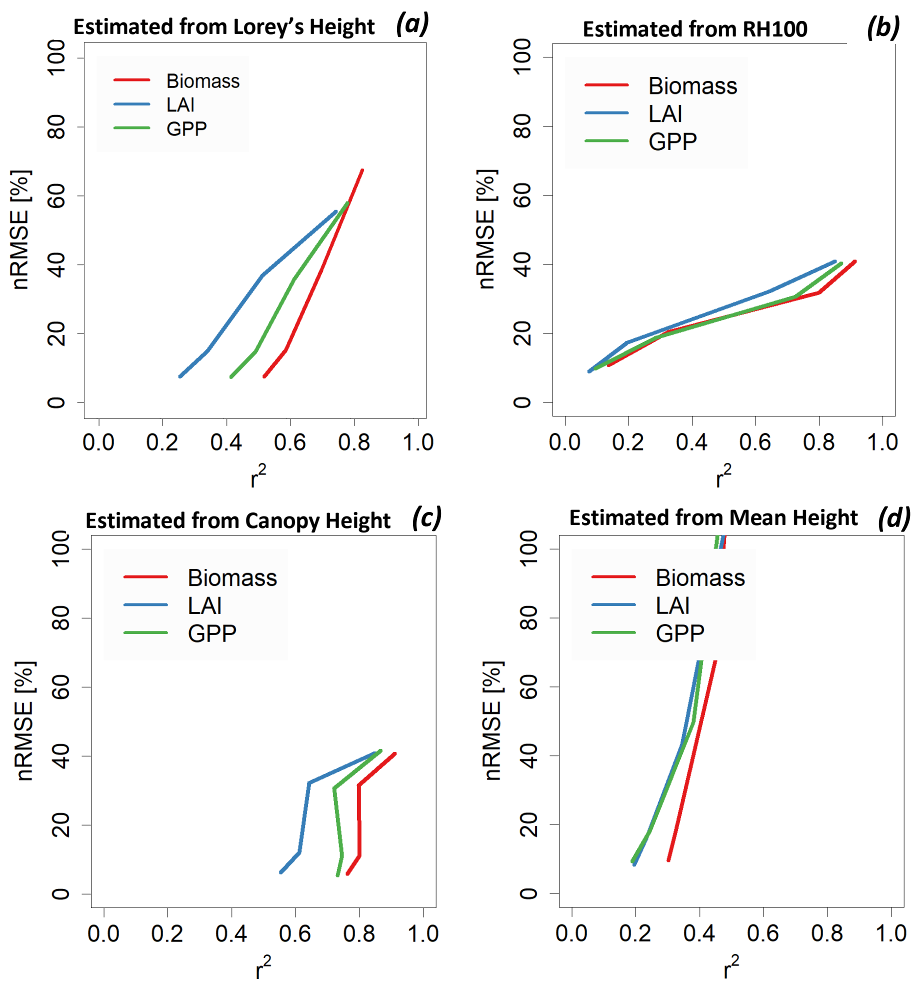

Figure F-1 *The figure summarizes the behavior of R^2 vs normalized root mean square error (nRMSE) for each of the correlations by each height definition, such that: (a) is Lorey's Height, (b) us RH100, (c) is canopy height and (d) is mean height. Biomass is shown in red, LAI is shown in blue and GPP is shown in green for all figures.*

Canopy height had the smallest range in R^2 values between resolutions across each variable tested. For example, AGB had a less than 20% difference while the range in nRMSE was ~30%. This is compared to an 80% difference in R^2 for RH100 (similar nRMSE difference) and a 40% (nRMSE difference: 50%) for Lorey's height. The LAI and GPP R^2 to nRMSE relationships have similar line shapes to that of AGB in the canopy height (F-1, c) and RH100 (F-1, b) plots, with a slightly larger R^2 range for LAI and slightly smaller R^2 range for GPP for canopy height. The proximity of the lines in to the lower right quadrant for canopy height and high resolution RH100 points indicates that both height metrics relate best to AGB, LAI and GPP. In both cases, the 20m plot resolution exhibits the demonstrably best accuracy/precision balance. This finding is supported by the knowledge that the typical diameter of a mature canopy tree crown is 20m in tropical rainforest ecosystems.